Received: 28 May 2023 | Revised: 9 July 2023 | Accepted: 10 July 2023

DOI: 10.1002/pol.20230342

RESEARCH ARTICLE

JOURNAL OF POLYMER SCIENCE WILEY

Macroporous fibers electrospun from dual-good solvent system

Fang-Ting Chen | Kai-Pin Chang | Yi-Cheng Liao | Shih-Huang Tung

Institute of Polymer Science and Engineering, National Taiwan University, Taipei, Taiwan

Correspondence
Shih-Huang Tung, Institute of Polymer Science and Engineering, National Taiwan University, Taipei 106319, Taiwan.
Email: shtung@ntu.edu.tw

Funding information
National Science and Technology Council, Taiwan, Grant/Award Numbers: 111-2622-8-007-011, 109-2221-E-002-182-MY3

Abstract

The polymer/solvent/nonsolvent ternary solutions have been previously used for fabricating electrospun macroporous fibers, in which the nonsolvent was expected to induce a liquid–liquid phase separation that leads to formation of pores after drying. In this study, we demonstrate that the poly(styrene-*co*-acrylonitrile) (SAN)/chlorobenzene (CB)/dimethyl sulfoxide (DMSO) system can be successfully electrospun into highly uniform macroporous fibers with pore size >50 nm at CB/DMSO volume ratio ~7/3 though both CB and DMSO are good solvents to SAN. The results imply that a premixed nonsolvent is not necessary for the formation of macropores. We find that it is the water droplets condensed from the atmosphere that work as the nucleation sites to trigger the phase separation while water-miscible DMSO plays a supporting role to expand the solvent-rich phase and the resultant pore size. Instead of solvent quality, the distinct volatilities and water miscibilities of the solvents are the keys. The macropores throughout the fibers provide high surface areas and large openings on surface such that the fibers show a significant improvement in oil adsorption capacity in comparison to the smooth and mesoporous ones.

KEYWORDS

breath figure, electrospinning, oil adsorption, porous fibers, vapor-induced phase separation

1 | INTRODUCTION

Porous polymeric materials composed of interconnected or closed pores have low relative density, high specific surface area (SSA), and good permeability, widely used in filtration, separation, adsorption, catalysis, insulation, and drug release.[1–3] Liquid–liquid phase separation techniques are commonly adopted in fabrication of porous polymeric materials, especially porous membranes.[4–7] In these techniques, the polymer solutions are demixed into polymer-rich phases and solvent-rich phases, which then leave the polymer skeleton and pores, respectively, after solidification. The liquid–liquid phase separation is primarily divided into three categories based on the mechanisms: nonsolvent-induced phase separation (NIPS), thermally-induced phase separation (TIPS), and vapor-induced phase separation (VIPS).[5,8–10] In addition to the phase separation techniques, the breath figure (BF) method in which the regularly-arranged water droplets condensed from atmosphere work as templates has widely been used to fabricate ordered porous films.[11–14] Apart from membranes or films, the liquid–liquid phase separation and BF techniques have been applied to electrospinning for preparing porous fibers.[15–19] In NIPS, the phase separation is induced either by premixed nonsolvents[20–25] or by post-treatment with nonsolvents.[26–28] For the TIPS method, the solvent quality is turned to be poorer to polymers by lowering the temperature to cause a phase separation.[29–31] VIPS requires solvents with low volatility and high water-miscibility such that the condensed water dissolves in

solutions and serves as the nonsolvent.[32–35] BF generally uses high volatile and water-immiscible solvents that can stabilize the water droplets on solution surfaces, thus mostly leaving pores on fiber surface only.[15,36,37]

The use of NIPS to produce porous electrospun fibers with the addition of nonsolvent to induce phase separation often leads to the instability of liquid jets and results in nonuniform fibers of varying diameters and irregular porous structures.[20–23] We have previously reported that the ternary solution of polystyrene (PS)/CB/DMSO can be electrospun into macroporous electrospun fibers with uniform fiber diameter and pore size, which shows an excellent oil adsorption capability.[38] The macropores are defined as the pores with width >50 nm here.[39] CB is a good solvent and DMSO is a nonsolvent to PS, respectively, and this combination happens to be suitable for electrospinning of macroporous fibers. The ratio of CB/DMSO and the relatively humidity were found to significantly affect the porous structures. Recently, we further used polylactide (PLA) coupled with different pairs of good solvents and nonsolvents to clarify the pore formation mechanism during electrospinning.[40] We concluded that uniform macroporous fibers can only be obtained under the following specific conditions: (i) the good solvent must be immiscible with water and of a boiling point higher than 100 °C; (ii) the nonsolvent must be miscible with water and must be highly polar (dielectric constant >35); (iii) the boiling point of the nonsolvent must be 20 °C higher than that of the good solvent.

In this work, the copolymer SAN was used for electrospinning. The SAN fibers with smooth surface had been previously electrospun from solutions of single solvent[41,42] and the application in enzyme immobilization had been demonstrated.[43] Here, the solutions were prepared by dissolution of SAN in the cosolvent of CB and DMSO. Unlike the conventional good solvent/nonsolvent pairs, the water-immiscible CB and water-miscible DMSO are both good solvents to SAN due to the amphiphilic nature of SAN. Surprisingly, this dual good solvent system can produce highly uniform macroporous fibers at specific CB/DMSO ratio, ~7/3, in a simple one-step process. In other words, different from the previous argument, the water-miscible, high-boiling solvent is not necessary to be a nonsolvent for triggering phase separation. This is therefore not a NIPS mechanism.

We systematically investigated the effects of the solvent composition and the humidity on fiber morphology, and find that this is a process combining the BF and VIPS mechanisms, as a result of the distinct volatilities and water miscibilities of CB and DMSO. It takes the advantage of the BF method, in which water vapor condenses on the surface of the hydrophobic polymer solutions (mostly CB) to form evenly distributed water droplets that serve as the nucleation sites for the growth of pores.[14,44] It also involves the VIPS technique, where the inter-mixing of the water-miscible solvent (DMSO) and the condensed water, a nonsolvent to SAN, induces the phase separation.[10,15,45,46] Furthermore, the diffusion of DMSO into water droplets expands the solvent-rich phases, allowing the pores to extend into the interior of the fibers, which greatly increases the SSA of the fibers. Along with the large openings of the pores on the surface that facilitate the infiltration of liquids into the fibers, the macroporous fibers show a superior oil adsorption capacity in comparison to the smooth and mesoporous counterparts. The method is simple and highly effective to fabricate porous electrospun fiber and to the best of our knowledge, this is a mechanism that has not been proposed yet.

2 | EXPERIMENTAL SECTION

2.1 | Materials

The copolymer, SAN (25 wt% acrylonitrile, M_W = 165,000 g/mol, and PDI = 1.67), was purchased from Sigma-Aldrich. The organic salt, tetrabutylammonium perchlorate (TBAP, >98%), was purchased from TCI. The solvents, CB (99.5%) and DMSO (99.9%), were purchased from J. T. Baker. All chemicals were used as received and the solvents were carefully stored in a desiccator to prevent absorption of water.

2.2 | Sample preparation

The solutions for electrospinning were prepared by mixing SAN in the cosolvents of CB and DMSO at various volume ratios, with and without 2.5% (wt/vol) TBAP to adjust the conductivity of the solutions. The concentration of SAN was between 100 and 450 mg/mL. The mixtures were magnetically stirred at 65 °C for 12 h to obtain homogeneous solutions, which were then cooled to room temperature for electrospinning. The electrospinning used a single-capillary spinneret, for which the solutions were fed into a syringe pump (YSP-301, YMC) that transported the solutions to a metallic needle (22 gauge, Hamilton) at a feed rate of 1.5 mL/h. A power supply (chargemaster VCM30-P, Simco-Ion) was connected to the metallic needle, providing a voltage of 10.9 kV for ejecting the solutions. The fibers were collected on aluminum foil or silicon wafer placed 19 cm below the tip of the needle without other treatments. The electrospinning was carried out at room temperature (23–28 °C) and at a relative humidity (RH) of 60%, unless otherwise specified.

2.3 | Scanning electron microscopy

The morphologies of fibers were characterized by a JEOL JSM-6330F field-emission scanning electron microscopy (SEM) at an accelerating voltage of 10 kV. The samples were sputtered with platinum by a JEOL JFC-1600 coater before imaging. For imaging the cross-sections, the fibers were collected on silicon wafer in the electrospinning process and then sputtered with platinum. After sputtering, the wafers with attached fibers were immersed in liquid nitrogen where they were broken into pieces to reveal the fiber cross-sections for imaging.

2.4 | Mercury intrusion porosimetry

The pore size distribution, porosity, and SSA of fibrous mats were determined by a mercury porosimeter (AutoPore IV 9520, Micromeritics). The volumes of pores at corresponding sizes were measured based on the volume of the intruded mercury under pressure (P). The samples were equilibrated at each pressure for 15 s in the range between 0.1 and 60,000 psia. The pressure was converted to pore diameter (D) assuming cylindrical pore geometry by the Washburn equation[47]

$$D = \frac{-4\gamma\cos\theta}{P} \quad (1)$$

where the surface tension (γ) of mercury is 485 dyn/cm and the contact angle (θ) is 130°. The cumulative specific intrusion volume (V) of mercury as a function of D was determined and the pore size distribution curve is expressed as dV/dD against D.

2.5 | Oil adsorption

Approximate 10 mg of fibrous sorbents collected from the aluminum foil was immersed in 40 mL motor oil in a glass beaker. After 1 h adsorption, the sorbents were removed from the oil bath and drained for 10 min. The oil adsorption Q (g/g) of the fibrous sorbents was calculated by

$$Q = \frac{w - w_0}{w_0} \quad (2)$$

where w_0 is the weight of the sorbent before adsorption and w is the total weight of the sorbent after adsorption and draining. Each sample was independently measured for at least three times.

3 | RESULTS AND DISCUSSION

3.1 | Electrospinnability

SAN can fully dissolve and form transparent solutions at concentration above 450 mg/mL in both neat CB and DMSO as well as in their cosolvents at all the CB/DMSO volume ratios, indicating that neither CB nor DMSO is nonsolvent to SAN. A series of SAN solutions at various CB/DMSO ratios and at SAN concentrations ranging from 100 to 450 mg/mL were used to examine the electrospinnability of the solutions at a RH of 60%. The solution viscosity was in the range between 0.054 and 10.143 Pa s. The large-area SEM images of the resulting electrospun products are shown in Figure 1 and the dependence of the morphology on SAN concentration and DMSO volume fraction in the cosolvents is plotted in Figure 2. A sufficient amount of DMSO in the cosolvents is required for successful electrospinning. At the DMSO fractions below 10%, the ejection of the liquid jets from Taylor cone is unstable due to the low dielectric constant of CB, which manifests one of the important roles of DMSO, that is, to increase the electrical conductivity (σ) of the solutions. The σs of CB and DMSO are 1.2×10^{-11} and 3×10^{-8} S/cm, respectively.[48,49] At low SAN concentrations, the polymer chains are less entangled and only spherical beads are collected. As SAN concentration increases, the beads are first elongated into spindle-like in shape and coexist with fibers, and then turn to be uniform fibers. The average fiber diameter increases with SAN concentration, ranging from 200 nm to 9 μm, as shown in Figure S1. At SAN concentrations above 450 mg/mL, the solutions are too viscous to be pumped to the syringe needle for electrospinning.

The morphologies of the fibers are dependent on the cosolvent composition. The closer views of the fiber surfaces and cross-sections at SAN concentration >200 mg/mL are shown in Figures S2 and S3, respectively. The representative SEM images for CB/DMSO = 9/1, 7/3, 6/4, and 1/9 at a SAN concentration of 400 mg/mL are displayed in Figure 3. At CB/DMSO = 9/1, small pores are seen on the fiber surface and the pore size expands underneath the surface, which is analogous to the porous structure created by the BF method using water-immiscible solvents.[15,36] The size and depth of the pores increase with DMSO fraction till CB/DMSO = 7/3 where larger pores appear on the surface and the pores extend deeply to the core of the fiber. At CB/DMSO = 6/4, the fiber surface becomes rough, caused by the large irregular pores and long grooves, and small holes are formed inside the fiber. As DMSO fraction keeps increasing, the fiber surface is smoother and only small holes are seen inside the fiber, as shown in the 1/9 case. This is typical of the

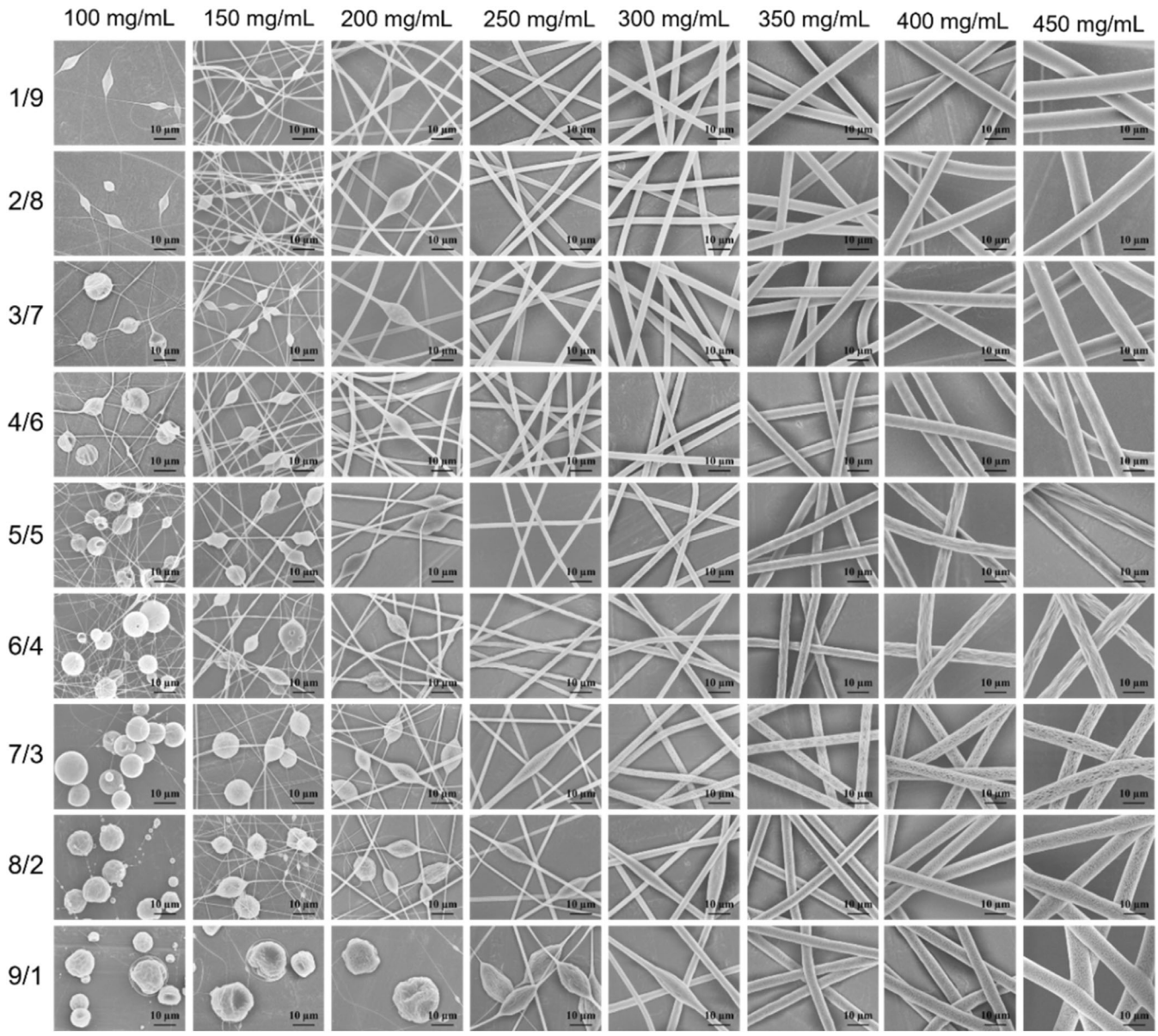

FIGURE 1 SEM images of the products electrospun from the SAN/CB/DMSO systems at varying SAN concentrations and CB/DMSO volume ratios. The scale bars are all 10 μm. CB, chlorobenzene; DMSO, dimethyl sulfoxide; SAN, poly(styrene-*co*-acrylonitrile); SEM, scanning electron microscopy.

porous fiber produced by the VIPS method in which water-miscible solvents are used.[10,50] The variation of the fiber morphologies with the cosolvent composition results from different pore formation mechanisms and the ratio of CB/DMSO = 7/3 is optimal for fabricating macroporous fibers.

3.2 | Effects of humidity

The change in the morphology of the electrospun fibers with RH at CB/DMSO = 9/1 are shown in Figure 4. The SAN concentration was fixed at 350 mg/mL. At a low RH of 40%, small and sparse pores appear on the fiber surface and only exist in the skin layer of the fibers. As RH increases, more surface pores are formed and the size is slightly increased while the holes inside the fiber are greatly expanded and penetrate deeper into the core. At RH = 80%, the holes inside the fiber are over 1 μm, with more than one small openings on the surface for each hole. In addition to the pore size, the fiber diameter increases with RH, mainly because of the higher vacancy inside the fiber that causes an expansion in total volume. Similar phenomenon is observed for CB/DMSO = 7/3 (Figure S4). The pores on the fibers are shallower and irregular at RH = 40% though are larger than those for

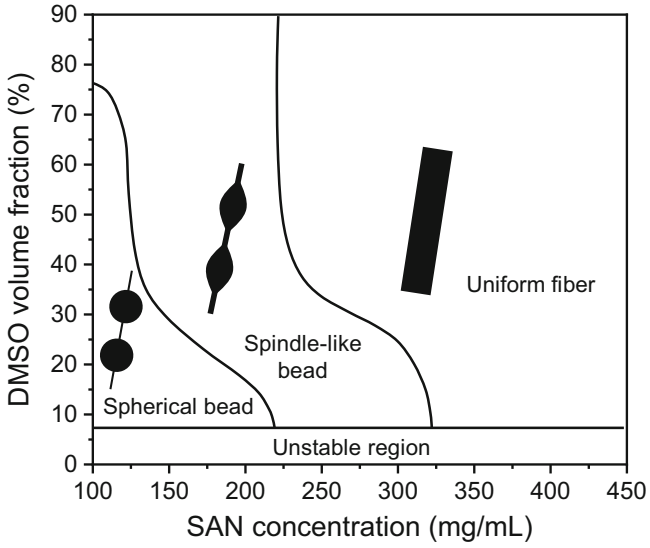

FIGURE 2 Electrospinnability of the SAN/CB/DMSO system. CB, chlorobenzene; DMSO, dimethyl sulfoxide; SAN, poly(styrene-*co*-acrylonitrile).

CB/DMSO = 9/1 at the same RH. At RH above 60%, pores are clearly seen on the surface and inside the fibers. The pore size and fiber diameter at RH = 80% are both larger than those at 60%. In the case of CB/DMSO = 5/5 (Figure S5), although the pores are invisible on the rugged surface, the size of the holes inside the fibers and the fiber diameter also both increase with RH. These results highlight the importance of the ambient water vapor in the formation of the pores.

3.3 | Mechanism

Uniform macroporous electrospun fibers have been shown to be successfully fabricated from the ternary solutions where the solvents are both good solvents to the polymer. Such macroporous structure on fibers has to result from a liquid–liquid phase separation of the polymer solution during electrospinning, but apparently not induced by either of the solvents. As revealed in the preceding section, the ambient moisture greatly affects the porous structure on fibers. The earlier evaporation of the lower-boiling solvent, CB, during electrospinning cools the liquid jet, which causes water vapor to condense. Water is a nonsolvent to SAN and the condensed water must be crucial for the occurrence of the phase separation in this system. If the solvent is not miscible with water, the condensed water forms isolated droplets stabilized by the polymer on the surface of liquid jets, leaving pores on fiber surface only after solidification, which is the well-known BF process and is the case for the fibers electrospun from the cosolvents of a much higher fraction of

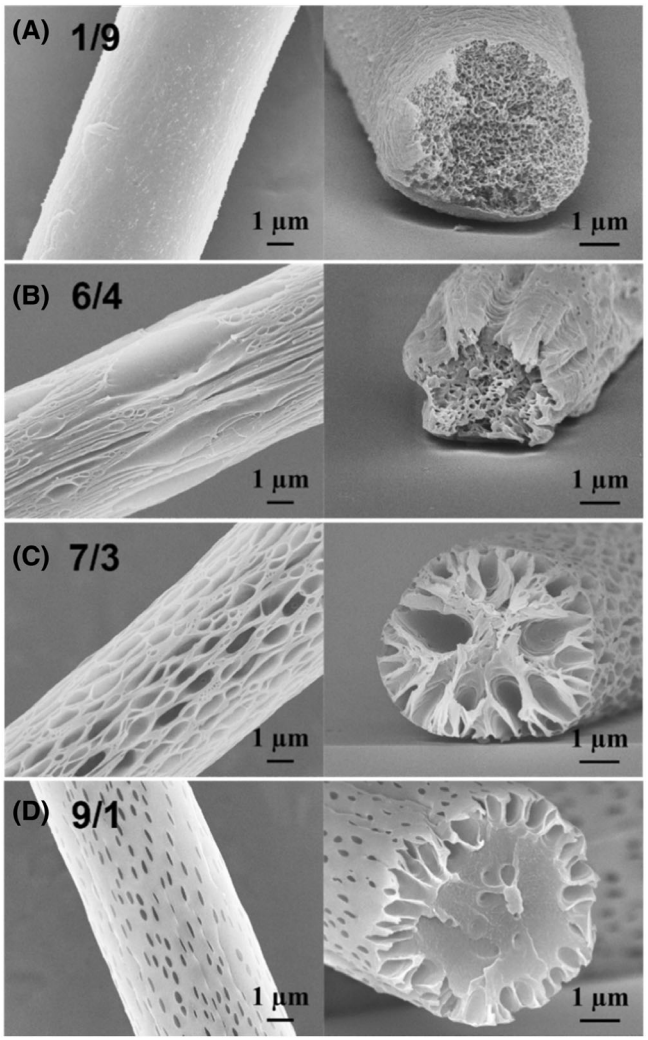

FIGURE 3 Representative SEM images of the fiber surfaces and cross-sections electrospun at CB/DMSO = (A) 1/9, (B) 6/4, (C) 7/3, and (D) 9/1. The SAN concentration is 400 mg/mL. CB, chlorobenzene; DMSO, dimethyl sulfoxide; SAN, poly(styrene-*co*-acrylonitrile); SEM, scanning electron microscopy.

water-immiscible CB, namely CB/DMSO = 9/1 and 8/2 (Figure 3 and Figure S3). For the cosolvents with the DMSO fraction above 60%, due to the high water-miscibility of DMSO, the condensed water can mix into the solution rapidly, which induces the phase separation inside the liquid jet and thus leads to small holes inside the fibers. This mechanism is known as VIPS.

For CB/DMSO around 7/3 that is optimal to produce macroporous fibers, the cosolvent is hydrophobic enough for the condensed water to maintain as droplets on the solution surface, stabilized by SAN molecules at the water/solvent interfaces. Because of the high affinity with water, DMSO in the solution tends to diffuse into the water droplets and the homogeneously mixed DMSO/water solvent then works as the nonsolvent to induce the phase separation. In other words, the water

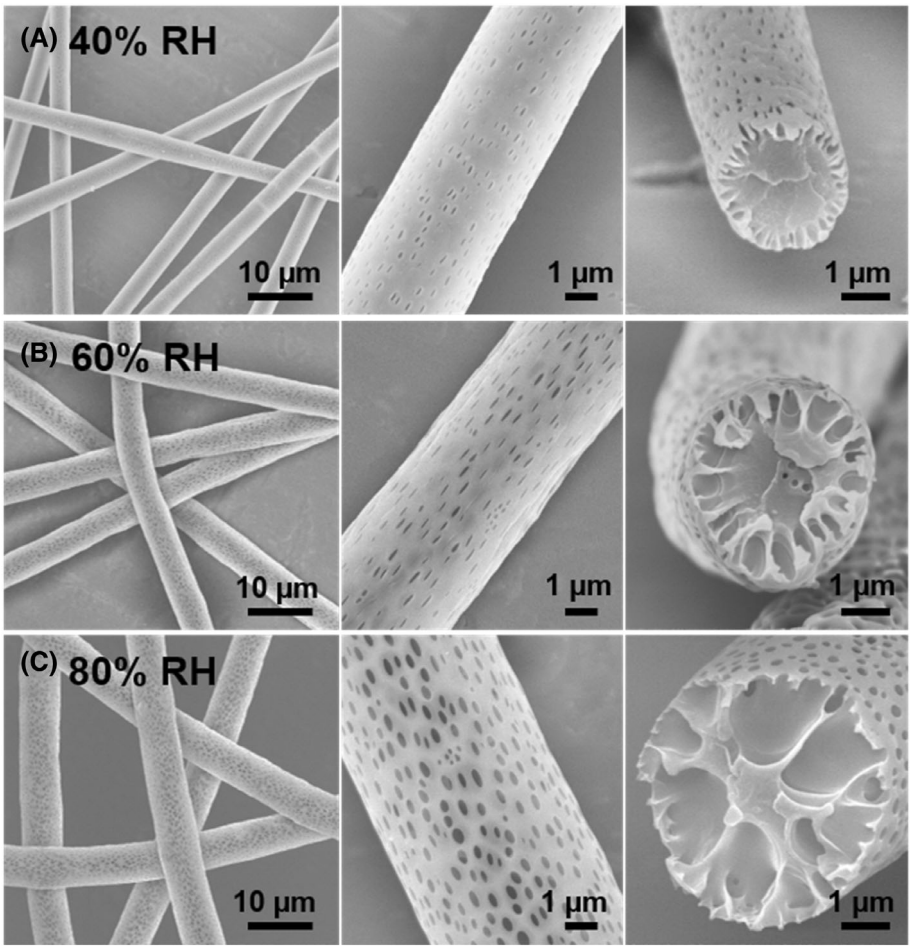

FIGURE 4 SEM images of the fibers electrospun at RH of (A) 40%, (B) 60%, and (C) 80%. The CB/DMSO ratio is 9/1 and the SAN concentration is 350 mg/mL. CB, chlorobenzene; DMSO, dimethyl sulfoxide; SAN, poly(styrene-*co*-acrylonitrile).

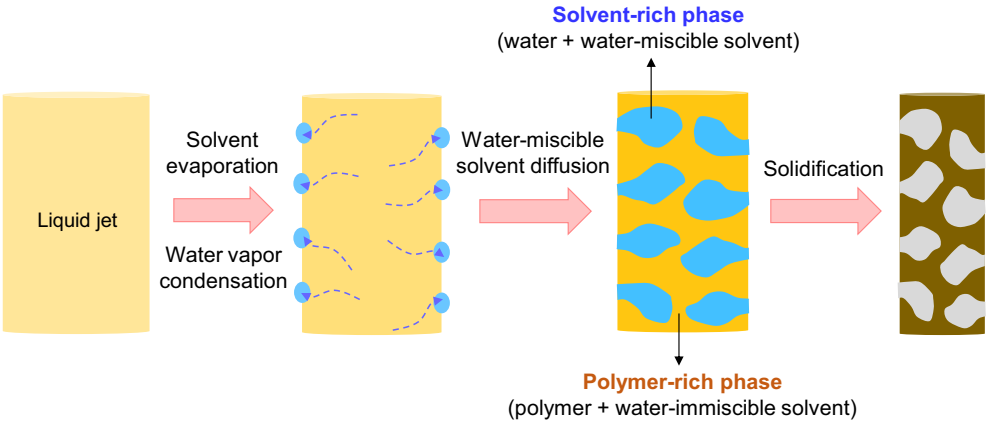

FIGURE 5 Formation mechanism of the macroporous fibers during electrospinning by the water-miscible solvent-assistant breath figure (WMSBF) method.

droplets are the nucleation sites for the solvent-rich phases. The DMSO/water mixed solvent is the major component in the solvent-rich phases which is extended from surface into the interior of the liquid jet as DMSO continuously diffuses into the droplets. The polymer-rich phases are mainly composed of SAN and CB. The extended solvent-rich phases then form the deep macropores on the SAN fibers after drying. This process is illustrated in Figure 5, which is a combination of the BF and VIPS mechanisms. Specifically, it is a BF method with additional water-miscible solvent that facilitates phase separation to create pores throughout the fibers. For convenient reason, we term this method as water-miscible solvent-assistant breath figure (WMSBF). In addition to the CB/DMSO pair, we find that the solutions of SAN in CB/dimethylformamide (DMF) cosolvent can also be used to produce macroporous fibers but at a higher RH of 80%, as shown in Figure S6, possibly due to the lower water affinity and higher volatility of DMF compared to DMSO. An analogous system of PMMA/dichloromethane

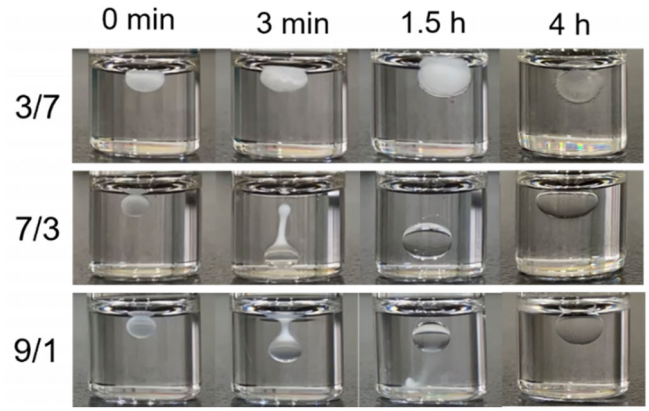

FIGURE 6 Representative photographs for the changes of 10 μL water droplets with time on the SAN solutions at CB/DMSO = 3/7, 7/3, and 9/1. The SAN concentration is 350 mg/mL. CB, chlorobenzene; DMSO, dimethyl sulfoxide; SAN, poly(styrene-*co*-acrylonitrile).

(DCM)/DMF has been electrospun into fibers with porous interiors and surfaces, previously attributed to the VIPS mechanism,[9] where both DCM and DMF are good solvents to PMMA. Although the pores on the PMMA fibers are smaller and less uniform compared to the present system due to higher volatilities of DCM and DMF,[40] the pore formation can be well explained by the WMSBF mechanism.

To prove the argument about the diffusion of DMSO into the condensed water droplets, 10 μL water was intentionally dropped onto the SAN solutions (350 mg/mL) at CB/DMSO = 3/7, 7/3, and 9/1 to mimic water condensed on liquid jets. The selective photographs for the changes of the water droplets with time are shown in Figure 6 and the complete photographs are shown in Figure S7. For the 9/1 and 7/3 solutions, the droplets grow with time and remain stable in these CB-rich solutions after 4 h though they sink and rise in the solutions due to the density changes. This is attributed to the continuous diffusion of DMSO into the droplets that are stabilized by SAN molecules locating at the interfaces. The droplet size in the 7/3 solution is larger than that in the 9/1 solution because a greater amount of DMSO diffuses into the droplets. In contrast, for the hydrophilic 3/7 solution, water can more rapidly diffuse into the solution near the surface and thus causes a phase separation that leads the formation of a SAN cluster. The cluster slightly increases in size with time and becomes blurred after 4 h. It is possible that water gradually diffuses into the solutions and is locally diluted around the cluster, which in turn increases the solvent quality to SAN and thus causes a dissolution of SAN back to solutions. Although the time scale in the electrospun process is much shorter than that in this macroscopic experiment, considering that the diffusion time for the sub-micrometer-scaled phase separation in the liquid jets is rather short, the phenomenon found here can be a rational reference to qualitatively explain the pore formation on electrospun fibers.

3.4 | Morphology control and oil adsorption application

In addition to the CB/DMSO ratio and humidity as aforementioned, the fiber diameter and the porous structure can be tuned by incorporating the organic salt, TBAP, into the solutions. Figure S8 compares the fibers electrospun from the solutions at CB/DMSO = 7/3 with and without 2.5 mg/mL of TBAP. The fiber diameter becomes thinner and the pores are elongated in the presence of TBAP, implying a stronger stretching force during electrospinning. This results from the higher dielectric constant of the solution caused by TBAP. Furthermore, SAN in neat CB can be successfully electrospun into smooth fibers when TBAP is added, which is otherwise not electrospinnable due to the low dielectric constant of CB (Figure 2). By varying the electrospinning parameters, including CB/DMSO ratio and TBAP addition, the fibers with different structures and diameters were fabricated for a comparison of properties. The sample names of the fibers and their characteristics are listed in Table 1. The SEM images of the fibers are shown in Figure 7. D0-T fiber is thick and smooth without pores; D3 and D3-T are thick and thin fibers with deep macropores, respectively, both by the WMSBF mechanism; D7-T is thin fiber with small holes via the VIPS mechanism.

The mercury porosimetry was used to quantify the porous structures of the fibers in the form of nonwoven mats collected after electrospinning. The data are shown in Figure 8. In the fibrous mats, there are two spaces where mercury can penetrate under pressure: the gaps between fibers and the pores on fibers. As expected, the porous fibers (D3, D3-T, and D7-T) exhibit multimodal pore size distributions, in which the largest one is from the gaps between fibers and the others are from the pores on fibers. In contrast, the smooth D0-T fibers have only one distribution from the inter-fiber gaps. The peaks above 10^3 nm are the average sizes of the gaps between the fibers. The gaps of the thicker fibers, that is, D0-T and D3, are larger, close to 10^4 nm, while those of the thinner fibers, D3-T and D7-T, are smaller, around 10^3 nm. The peaks below 10^3 nm reflect the pore sizes on fibers. The macroporous D3 and D3-T fibers show pore sizes dominantly between 10^2 and 10^3 nm while D7-T show small pore sizes between 10^1 and 10^2 nm, consistent with the SEM images (Figure 7). The porosities and SSAs of the fibrous mats are listed in Table 1. The porosities vary slightly, ranging between 86% and 94%, among

TABLE 1 Preparation and characteristics of the fibrous mats shown in Figure 7.

Sample	CB/DMSO	SAN conc. (mg/mL)	TBAP (mg/mL)	Diameter (μm)	Porosity (%)	SSA (m^2/g)
D0-T	10/0	375	2.5	3.29 ± 0.25	86.42	2.36
D3	7/3	300	0	3.10 ± 0.21	93.45	11.31
D3-T	7/3	300	2.5	1.18 ± 0.07	91.14	26.21
D7-T	3/7	300	2.5	1.21 ± 0.07	93.00	50.11

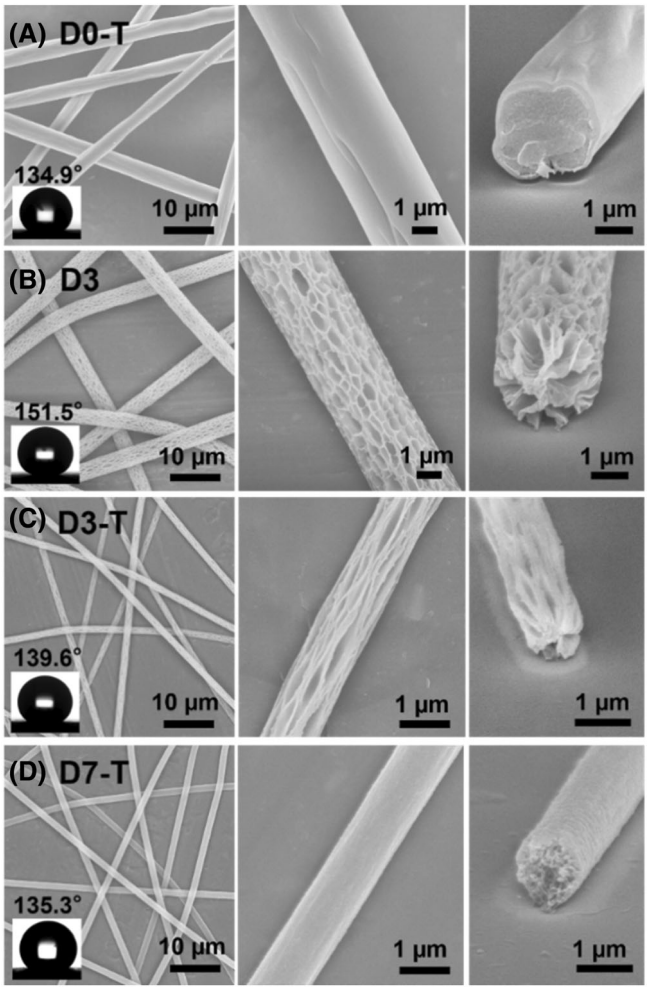

FIGURE 7 Scanning electron microscopy images of (A) D0-T, (B) D3, (C) D3-T, and (D) D7-T fibers prepared for the mercury porosimetry measurements and oil adsorption tests. The insets are the photographs of the water contact angle measurements.

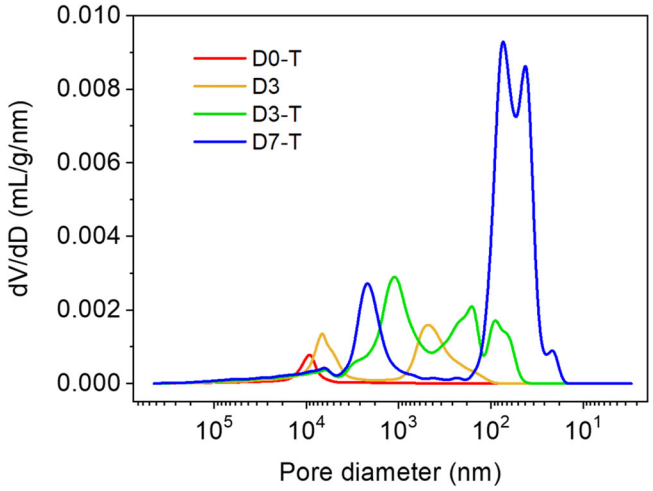

FIGURE 8 Pore size distributions of the fibrous mats shown in Figure 7 determined by the mercury porosimetry.

which D0-T shows relatively lower porosity. In contrast, the SSAs of the fibers are significantly different. The SSA of the thick, smooth D0-T is expectedly the lowest, only 2.36 m^2/g. Porous structures and thinner fiber diameters can effectively create the surface area. D3 shows a higher SSA of 11.31 m^2/g and that of D3-T greatly increases to 26.21 m^2/g. Because of the nanoscaled holes well dispersed in the fibers, D7-T exhibits the highest SSA, up to 50.11 m^2/g.

The water contact angle of the smooth SAN film is 80.1 ± 1.2° and those of D0-T, D3, D3-T, and D7-7 fibrous mats are increased to 134.9 ± 3.2°, 151.5 ± 0.6°, 139.6 ± 2.8°, and 135.3 ± 2.4°, respectively, as shown in the insets of Figure 7, due to the presence of the inter-fiber gaps and the pores that can trap air. The porous fibrous mats are thus hydrophobic in nature and can selectively adsorb oil while repel water, suitable for oil–water separation.[33] Here, the four fibrous mats discussed above were applied in oil adsorption and the effects of the fiber morphology on the adsorption capacity was investigated. The motor oil with a viscosity ~0.2 Pa s was used in this experiment. The maximum adsorption capacities of the fibrous mats are compared in Figure 9, which reveals the order of D3-T > D7-T > D3 > D0-T. The adsorption capacity of the thin, macroporous D3-T fibers is 218 g/g, much higher than those of others, among which the adsorption of the thick, smooth D0-T fibers is the lowest, only 47 g/g. The oil adsorbed into fibers is distributed in both the gaps between fibers and the pores on fibers,[33,38] driven by the capillary action to reduce the surface free energy of fibers. Therefore, thinner and porous fibers with larger surface areas are more effective for oil adsorption. Moreover, larger pores are beneficial for the penetration of oil, which explains why the adsorption capacity of D3-T is higher

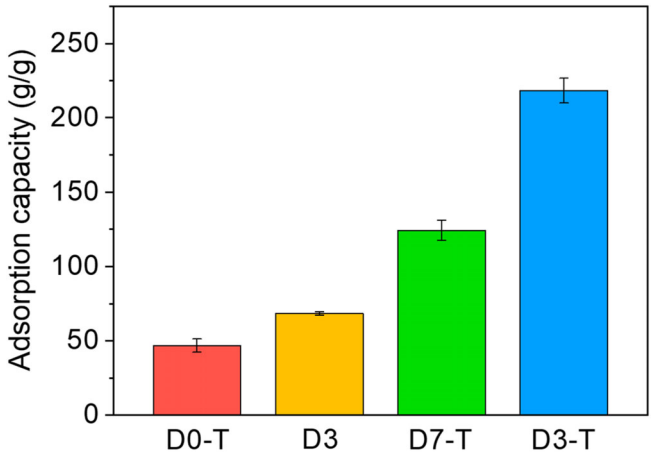

FIGURE 9 Maximum oil adsorption capacities of the fibrous mats shown in Figure 7. The motor oil was used.

than that of D7-T with mesoscale holes mostly less than 50 nm though D7-T has the highest SSA. The low capacity of D3 with macropores is mainly due to the thicker fiber diameter that lowers the SSA, but it is still higher than that of the smooth D0-T with a similar fiber diameter. The oil adsorption capacities as functions of time for D0-T and D3-T fibers are compared in Figure S9. D3-T not only shows a higher maximum capacity but also a higher adsorption rate at the initial stage.

The oil adsorption capacities of porous electrospun fibers in the previous reports were generally in the range between 100 and 200 g/g[15,33] and in some particular cases, the capacity reached 800 g/g or above.[38,40] Because the hydrophobicity of polymers, sorbent compactness that depends on the ways to collect fibers, and the draining time in the adsorption experiments may greatly affect the adsorption capacity, it is difficult to make an objective comparison of the capacities between the previous and present results. However, from the above systematic comparison of the SAN fibrous mats under the same test conditions, the macropores created by this simple electrospinning process are demonstrated to be highly advantageous for oil adsorption.

4 | CONCLUSIONS

In this work, different from the conventional viewpoint that a premixed nonsolvent is required in ternary systems to prepare macroporous electrospun fibers, we show that the cosolvent composed of two good solvents, CB and DMSO, can be used to electrospin the copolymer, SAN, into uniform fibers with evenly distributed macropores throughout the fibers that exhibit improved oil adsorption capacity. The previously proposed NIPS mechanism used to explain the formation of pores in these systems should therefore be modified. Based on the results of our previous[40] and present works, we suggest that to meet the criterion for electrospinning of macroporous fibers, the solvent quality is not a decisive factor and instead, the two solvents need to have distinct volatilities and water miscibilities. The characteristics and roles of the solvents are summarized as follows: (i) the water-immiscible solvent must have a relatively low boiling point, and thus its evaporation can lower the temperature of the solution, causing water vapor to condense on the liquid surface; (ii) the water-miscible solvent must have a high boiling point, 20 °C higher than the water-immiscible solvent, and must have a high polarity (dielectric constant >35), to ensure that a sufficient amount of the water-miscible solvent diffuses into the water droplets during the drying process. This technique is a combination of BF and VIPS methods, and is an effective way to prepare macroporous fibers potential for applications.

ACKNOWLEDGMENT

This work was financially supported by the National Science and Technology Council (NSTC 109-2221-E-002-182-MY3 and 111-2622-8-007-011) in Taiwan.

ORCID

Shih-Huang Tung https://orcid.org/0000-0002-6787-4955

REFERENCES

[1] D. C. Wu, F. Xu, B. Sun, R. W. Fu, H. K. He, K. Matyjaszewski, *Chem. Rev.* **2012**, *112*, 3959.
[2] G. Couture, A. Alaaeddine, F. Boschet, B. Ameduri, *Prog. Polym. Sci.* **2011**, *36*, 1521.
[3] J. Song, B. W. Zhang, Z. H. Lu, Z. Y. Xing, T. Liu, W. Y. Wei, Q. Zia, K. W. Pan, R. H. Gong, L. M. Bian, Y. Li, J. S. Li, *ACS Appl. Mater. Interfaces* **2019**, *11*, 46261.
[4] B. S. Lalia, V. Kochkodan, R. Hashaikeh, N. Hilal, *Desalination* **2013**, *326*, 77.
[5] P. Vandewitte, P. J. Dijkstra, J. W. A. Vandenberg, J. Feijen, *J. Membr. Sci.* **1996**, *117*, 1.
[6] H. Y. N. Thi, B. T. D. Nguyen, J. F. Kim, *Membranes* **2021**, *11*, 19.
[7] T. Wen, Y. T. Gao, J. J. Zhou, J. Qiu, S. Wang, J. Loos, D. J. Wang, X. Dong, *ACS Macro Lett.* **2023**, *12*, 697.
[8] X. B. Dong, D. Lu, T. A. L. Harris, I. C. Escobar, *Membranes* **2021**, *11*, 309.
[9] L. Li, Z. Jiang, M. M. Li, R. S. Li, T. Fang, *RSC Adv.* **2014**, *4*, 52973.
[10] P. Lu, Y. N. Xia, *Langmuir* **2013**, *29*, 7070.
[11] S. Falak, B. Shin, D. Huh, *Nanomaterials* **2022**, *12*, 1055.
[12] M. Srinivasarao, D. Collings, A. Philips, S. Patel, *Science* **2001**, *292*, 79.
[13] A. Zhang, H. Bai, L. Li, *Chem. Rev.* **2015**, *115*, 9801.

[14] A. Munoz-Bonilla, M. Fernandez-Garcia, J. Rodriguez-Hernandez, *Prog. Polym. Sci.* **2014**, *39*, 510.
[15] C. Huang, N. L. Thomas, *Eur. Polym. J.* **2018**, *99*, 464.
[16] C. Huang, N. L. Thomas, *Polym. Rev.* **2020**, *60*, 595.
[17] J. Xue, T. Wu, Y. Dai, Y. Xia, *Chem. Rev.* **2019**, *119*, 5298.
[18] B. Zaarour, L. Zhu, X. Y. Jin, *ChemistrySelect* **2020**, *5*, 1335.
[19] X. Y. Cao, W. Chen, P. Zhao, Y. Y. Yang, D. G. Yu, *Polymer* **2022**, *14*, 3990.
[20] Z. Wei, Q. Zhang, L. Wang, X. Wang, S. Long, J. Yang, *Colloid Polym. Sci.* **2013**, *291*, 1293.
[21] Z. Qi, H. Yu, Y. Chen, M. Zhu, *Mater. Lett.* **2009**, *63*, 415.
[22] K. A. G. Katsogiannis, G. T. Vladisavljević, S. Georgiadou, *Eur. Polym. J.* **2015**, *69*, 284.
[23] E. Rezabeigi, M. Sta, M. Swain, J. McDonald, N. R. Demarquette, R. A. L. Drew, P. M. Wood-Adams, *J. Appl. Polym. Sci.* **2017**, *134*, 44862.
[24] A. Y. Jiang, Z. J. Pan, *J. Nanopart. Res.* **2020**, *22*, 239.
[25] L. G. Liu, J. H. He, *Therm. Sci.* **2017**, *21*, 1821.
[26] R. P. Tian, P. Zhang, R. H. Lv, B. Na, Q. X. Liu, Y. H. Ju, *RSC Adv.* **2015**, *5*, 37539.
[27] K. Nayani, H. Katepalli, C. S. Sharma, A. Sharma, S. Patil, R. Venkataraghavan, *Ind. Eng. Chem. Res.* **2012**, *51*, 1761.
[28] Y.-A. Seo, H. R. Pant, R. Nirmala, J.-H. Lee, K. G. Song, H. Y. Kim, *J. Porous Mater.* **2012**, *19*, 217.
[29] H.-H. Chang, K. Beltsios, Y.-H. Chen, D.-J. Lin, L.-P. Cheng, *J. Appl. Polym. Sci.* **2014**, *131*, 40374.
[30] J. T. McCann, M. Marquez, Y. Xia, *J. Am. Chem. Soc.* **2006**, *128*, 1436.
[31] X.-Y. Ye, F.-W. Lin, X.-J. Huang, H.-Q. Liang, Z.-K. Xu, *RSC Adv.* **2013**, *3*, 13851.
[32] S. Megelski, J. S. Stephens, D. B. Chase, J. F. Rabolt, *Macromolecules* **2002**, *35*, 8456.
[33] J. Wu, N. Wang, L. Wang, H. Dong, Y. Zhao, L. Jiang, *ACS Appl. Mater. Interfaces* **2012**, *4*, 3207.
[34] R. M. Nezarati, M. B. Eifert, E. Cosgriff-Hernandez, *Tissue Eng. Part C* **2013**, *19*, 810.
[35] C. L. Casper, J. S. Stephens, N. G. Tassi, D. B. Chase, J. F. Rabolt, *Macromolecules* **2004**, *37*, 573.
[36] L. Natarajan, J. New, A. Dasari, S. Z. Yu, M. A. Manan, *RSC Adv.* **2014**, *4*, 44082.
[37] M. Bognitzki, W. Czado, T. Frese, A. Schaper, M. Hellwig, M. Steinhart, A. Greiner, J. H. Wendorff, *Adv. Mater.* **2001**, *13*, 70.
[38] P.-Y. Chen, S.-H. Tung, *Macromolecules* **2017**, *50*, 2528.
[39] K. S. W. Sing, D. H. Everett, R. A. W. Haul, L. Moscou, R. A. Pierotti, J. Rouquerol, T. Siemieniewska, *Pure Appl. Chem.* **1985**, *57*, 603.
[40] Y.-R. Chen, H.-W. Chung, S.-H. Tung, *ACS Appl. Polym. Mater.* **2021**, *3*, 5096.
[41] T. Senthil, S. Anandhan, *J. Electrostat.* **2015**, *73*, 43.
[42] R. Caro-Briones, B. E. Garcia-Perez, H. Baez-Medina, E. San Martin-Martinez, G. Martinez-Mejia, R. Jimenez-Juarez, H. Martinez-Gutierrez, M. Corea, *J. Appl. Polym. Sci.* **2020**, *137*, 49166.
[43] M. R. El-Aassar, M. Shibraen, Y. R. Abdel-Fattah, A. A. Elzain, *Fibers Polym.* **2019**, *20*, 2268.
[44] L. S. Wan, J. W. Li, B. B. Ke, Z. K. Xu, *J. Am. Chem. Soc.* **2012**, *134*, 95.
[45] J. Zheng, H. Zhang, Z. Zhao, C. C. Han, *Polymer* **2012**, *53*, 546.
[46] H. Fashandi, M. Karimi, *Ind. Eng. Chem. Res.* **2014**, *53*, 235.
[47] E. W. Washburn, *Phys. Rev.* **1921**, *17*, 273.
[48] J. Hart, A. G. Mungall, *Can. J. Phys.* **1956**, *34*, 491.
[49] J. H. Exner, E. C. Steiner, *J. Am. Chem. Soc.* **1974**, *96*, 1782.
[50] P. K. Szewczyk, U. Stachewicz, *Adv. Colloid Interface Sci.* **2020**, *286*, 102315.

SUPPORTING INFORMATION

Additional supporting information can be found online in the Supporting Information section at the end of this article.

How to cite this article: F.-T. Chen, K.-P. Chang, Y.-C. Liao, S.-H. Tung, *J. Polym. Sci.* **2023**, *61*(20), 2539. https://doi.org/10.1002/pol.20230342